3D Printed Biomedical Prototypes: Dielectric and Optical Properties

A.S. Bhattacharyya[1, 2*]

Department of Metallurgical and Materials Engineering [1]
Centre of Excellence in Green and Efficient Energy Technology (CoE-GEET) [2]

Central University of Jharkhand, Ranchi 835 205, India
e-mail: 2006asb@gmail.com ; arnab.bhattacharya@cuj.ac.in

ABSTRACT
The dielectric and optical properties of materials are important when creating biomedical prototypes utilising additive manufacturing or 3D printing. For high-frequency devices, characteristics such as dielectric constant, resistivity, and dielectric loss are used. Piezoelectric materials, such as polymer ceramic composites, have a significant impact on diagnostics and bone healing. 3D printed lenses and other metamaterial-based optical elements are employed in imaging and sensing applications incorporating polarisation and plasmonic characteristics.

Keywords: 3D printing, dielectric, optical, diagnosis, sensors

1. Introduction

Rapid prototyping and additive manufacturing, sometimes referred to as 3D printing, are widely employed in the biomedical industry to produce titanium scaffolds for orthopaedic implants, biomedical prototypes, optical elements, and chip-based devices **[1-5]**. Stereolithography (SLA), digital light processing (DLP), fused filament fabrication (FFF), fused deposition modelling (FDM), and material jetting are low-cost and simple procedures for making unique, customised goods. Polymers such as poly (lactic acid), polycarbonate, polyamide, polydimethylsiloxane, polyethylene terephthalate glycol (PET-G), and different thermoplastic polyurethane filaments (TPU) are used in these processes **[6, 7]**. In addition, much research is being conducted on piezoelectric polymers (PVDF), composites, and piezoelectric ceramics (PZT, BTO)**[8].**

The dielectric and optical properties of 3D-printed biomedical prototypes, in addition to mechanical and thermal features, are critical for their use. **[9-11]**. The electronic conduction of the materials used in additive manufacturing must be checked for usage in prototypes. Because of their unpredictable behaviour at very low frequencies, 3D-printed biosensors require a wider gamut of frequencies to operate. High-frequency sensor operation necessitates more input power, raising the overall cost of the sensing system. Polymer-based flexible sensors have alleviated some of the impact **[12]**. However, optical components utilised in biomedical equipment, such as lenses and mirrors, necessitate exceedingly uniform surfaces. To overcome this difficulty, advanced 3D printing techniques are being deployed. SLA cures polymers utilising optical processes such as photopolymerization with UV lasers and digital light processing (DLP). The optical properties of the 3D-printed polarisation mirrors, beam splitters, optical whispering-gallery modes (WGM), waveguides, and sensors used in biomedical prototypes have a substantial impact on performance. **[13].** Taking into account all of these factors, this communication discusses the dielectric and optical properties of 3D-printed biomedical prototypes..

2. Dielectric properties

The dielectric strength E_ρ ($kV \cdot mm^{-1}$), surface/volume resistivity (ρ_s / ρ_v), and dielectric loss (tan $\boldsymbol{\delta}$) are the main dielectric parameters looked for in the 3D printed systems for the selection of materials. The breakdown voltage to thickness ratio, often known as the dielectric strength, demonstrates an object's ability to act as insulation. The relative

permittivity of a dielectric substance describes its polarizability. Capacitance is connected to electric susceptibility, which is the measurement of the ease of polarisation subject to an external electric field. Impedance analyzers are used to test dielectric properties, particularly at low frequencies where the measuring capacitor has high impedance. Dielectric loss refers to the loss in energy as the material gets heated in an alternating electric field. It is expressed tan $\boldsymbol{\delta}$ where $\boldsymbol{\delta}$ is the angle between the alternating field vector and the material's loss component.

The measuring device provides the circuit parameters – total capacitance (C_p) and its quality factor (Q). The relationship between these two parameters is described by **eq 1**, where R is the sample loss resistance. The total capacitance consists of the parasitic capacitance of the supply conductors of the electrodes (C_{par}) and the capacitance of the tested sample (C_s). given as $C_s = C_{par} - C_p$. The loss factor (tan δ) is then calculated from the data (Q) according to **eq 2**[14]**.**

$$Q = \omega C_p R \quad (1)$$

$$\tan\delta = 100\frac{C_p}{QC_s} \quad (2)$$

In order to incorporate 3D-printed circuit elements into high-voltage devices, it is necessary to comprehend the insulating properties of the printed materials. This is because printed dielectric matrices containing conductive or metallic traces and other electrical components have made additive manufacturing possible for complex three-dimensional designs. According to research on the dielectric breakdown of additively manufactured polymeric materials using the SLS, FDM, and SLA processes, printed insulators would likely be less desirable due to reduced dielectric strength when insulating plastics are needed in high voltage applications that demand high dielectric strength insulators and conventional subtractive machining processes are viable. As insulator complexity begins to exceed the capabilities of subtractive machining technologies, a printed insulator would be a more competitive option. Dielectric composites in the form of $BaTiO_3$ (BTO) microparticles were combined with ABS to make 3D-printed objects with high permittivity. The microwave dielectric properties found using a 15GHz split post-dielectric resonator were 2.6-8.7 and 0.005-0.027, respectively. The 3D-printed structures are depicted in Fig 1 [15-18].

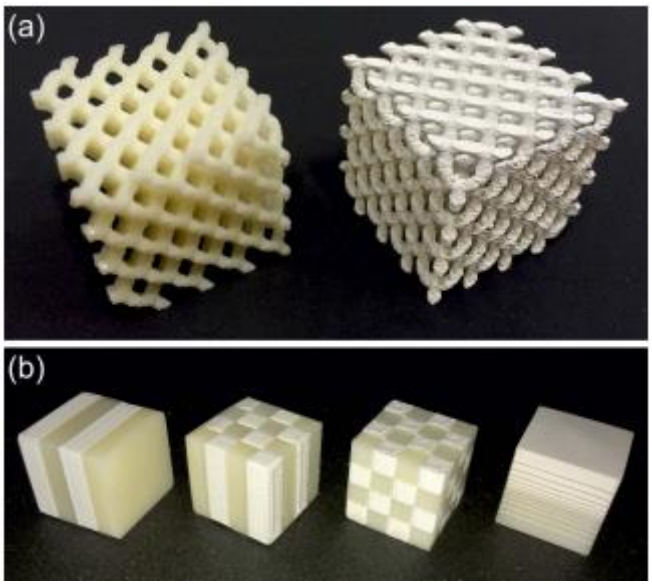

Fig 1: 3D-printed polymer composite parts. (a) rod-connected diamond photonic crystal structures printed in ABS polymer (left, ε' = 2.57) and 50wt% $BaTiO_3$/ABS polymer composite (right, ε' = 4.95). Scale: each cubic structure has an overall side length of 32mm (8mm unit cell). (b) 1D, 2D, and 3D periodic structures and a 1D graded structure printed using a combination of ABS polymer and 50wt% BaTiO3 in ABS polymer composite. Scale: each cubic structure has a side length of 16mm (**reproduced under CC-BY License – Open Access Castles**, F [18].

2.1 Electronic applications

Because they are affordable and have strong dielectric properties, PET-G and ABS-T are materials used in electronic applications. E is typically between 10 and 20 kV/mm for most polymers. However, thermoplastics showed higher values, whilst polymers with carbon fibre inclusions showed lower values. The semiconductive co-polymer ABS ESD has v = 3.58 108 cm and s = 4.38 108 cm when used as an encapsulating layer. [19]. The dielectric characteristics of 3D-printed PLA indicate good insulating qualities below the glass transition temperature. A dipolar relaxation mechanism and a significant change in the dielectric properties were found to occur during cold crystallisation. It can be quickly used to produce electrical components thanks to the addition of a small amount of the ionic liquid THTPT DE A small amount of the ionic liquid THTPT DE substantially increases PLA's conductivity, making it suitable for the fast production of electrical components. **[20].**

2.2 High-frequency applications

The dielectric properties of the 3D printing materials PLA, PET-G, and ABS showed that their relative permittivity varied between 2.9 and 4.2 MHz in the frequency range. The loss factors ranged from 0.8 to 4.0%. For electrical applications, ABS and PLA-Metallic Green are suitable materials due to their low-frequency dependence up to 70 MHz and their low loss coefficients (0.9-1.5%). **[14].**

For MRI, additive manufacturing can be used to create the structure of RF coils as well as other parts. The dielectric constant and loss tangent of 3D-printed polymers (ABS, PLA, and Methacrylate Photopolymer Resin, MPR) in the MRI frequency range (up to 300 MHz) have been examined in order to design and construct a receive-only RF coil that fits near to the body. **[21]**.

Resonant cavity, microstrip-line, and circular resonator approaches are used to explain the dielectric properties. Resonant procedures based on quantifiable shifts in resonance frequency and changes in the cavity's quality factor enable the most exact characterisation methods, especially for low-loss materials, although they can only be applied at microwave frequencies. **[22].**

2.4 Biosensors

A tiny, 3D-printed microwave probe has been used to calculate propagation losses and reflectometry within a biological medium acting as a biomedical antenna. The propagation losses for various human body regions have been considered for examination in human or animal bio-medical microwave testing. A paraffin and titanium oxide (TiO_2) high-dielectric material mixture can be used to create an elliptical double-ridged horn (EDRH) antenna for medical monitoring. The antenna has been designed and optimised to function in the frequency band (2–6 GHz) in order to accomplish high-resolution detection and maintain a WB. It is embedded in a high-dielectric material to reduce reflections brought on by a mismatch with the body and to further miniaturise the recommended antenna. Due to its 4 GHz bandwidth, amplification of 5-8 dB, and excellent impedance matching, it can function at lower frequencies and allow monitoring very deep into the human body. For use in biomedical applications, a monopole microstrip antenna with a curved substrate that has been manufactured in three dimensions (3D) has been developed. The thickness of abdomen fat is measured and verified using a pyramidal double-ridged horn antenna that was 3D printed and filled with a high dielectric substance. **[24 - 29].**

2.3 Piezoelectric properties

Using a Cu doped-ZnO reinforcement and a polyvinyl fluoride (PVDF) matrix with piezoelectric capabilities, low-cost non-enzymatic glucose smart biomedical sensors have been created. The amount of polarisation produced per unit of mechanical stress is measured by the piezoelectric constant, or Berlincourt metre, d33. Pico(10–12)

Coulomb/Newton (pC/N) is the unit. The polarisation causes the creation of dipole moments, which are measured in terms of their polarizability (pC cm^{-2}) per unit volume. The materials have a dielectric constant of 6.5 and a piezoelectric coefficient of 19.3 pC/N, which are suitable for bioreceptors and transducers. A flexible silver-coated PNN-PZT grid-composite with grid architecture based on a PDMS matrix was made using the direct ink writing approach, and it displayed an improved piezoelectric and electromechanical coupling coefficient. A flexible silver-coated PNN-PZT grid-composite with grid architecture based on a PDMS matrix was made using the direct ink writing approach, and it displayed an improved piezoelectric and electromechanical coupling coefficient. The most popular piezoelectric ceramic for 3D printing is lead zirconate titanate (PZT), which has a high piezoelectric coefficient and simple manufacturing piezoelectric constant (212-345 pC/N) and dielectric constant (760-1390). The alignment of the dipoles is enhanced when piezoelectric materials are heated to high temperatures, which can improve the electromechanical coupling of the piezoelectric ceramics. Additionally, the sintered PZT was incorporated to create a 2D array for the ultrasound transducer with a centre frequency of 2.24 MHz. **[30-34]**.

Lead-free piezoelectric ceramics have taken the place of lead-based products as a result of the rising demand for environmentally benign and non-toxic materials. **[35]**. With a maximum polarisation of 2.29 pC cm^{-2} and a piezoelectric constant of 60 pC/N, BTO are lead-free and have exceptional dielectric and piezoelectric characteristics. In turn, this leads to an optimised dielectric coefficient (d33), which was raised from 290 to 360 pC/N **[36]**, improving sinterability.

2.4 Bone healing

Piezoelectric materials are utilised to regulate the growth and regeneration of bone cells. 3D printed implantable materials encourage piezoelectric and bioactive activity to promote bone healing. Piezoelectric materials having ferroelectric properties are used to control the interaction between ions and salts in situ and modify the surface charge of biological components in physiological settings. These impacts affect protein adhesion and bone healing. The piezoelectric properties of bone can encourage self-healing by producing an electric signal during movement **[37–39]**.

There are two types of piezoelectric effects that can be used to activate bone: direct effects (mechanical stimulation) and indirect effects (electrical stimulation or energy harvesting). Piezoelectric material scaffolds can produce electric impulses using dynamically collected energy, stimulating bone cells and promoting their adherence to the scaffolds. **[40]**. Porous titanium scaffolds with piezoelectric BTO coating were used to trigger osteogenic differentiation based on the piezoelectric effect produced by low-intensity pulsed ultrasonic stimulation. **[41]**. Piezoelectric materials can be 3D printed to create complex-structured smart stimulatory scaffolds and bone stimulation implants in the future. **[42].**

3. **Optical Properties**

3.1 Imaging and Spectroscopy

Tissue-simulating phantoms are necessary for many optical imaging and spectroscopic applications. A variety of optical phantoms may now be produced using 3D printing and acrylonitrile butadiene styrene (ABS) filaments, which is a novel method of manufacturing objects with changing geometry **[43]**. Even gratings and other optical elements may benefit from the natural waviness of many 3D-printed objects in order to achieve a particular effect.

3.2 Polymer Glass lenses

The optical densities, transmittances, and thermal stabilities of polymer and glass optical lenses vary **[44]**. Injection moulding of polymer optical lenses is possible **[45]**, and novel inkjet printing methods based on polymeric nano droplets can be used to produce micro-lens arrays **[46]**. It has been claimed that a modified inkjet printing technology was used to create a 3D printed lens with a 25 nm aperture **[47]**. For printed circuit boards (PCB), 3D printed polylactic acid (PLA) laser lenses with anti-reflected (AR) properties have been created using the hyperbolic lens equation using a 3D model as shown in **Fig. 2a**, where the wall height h =

/4n$^{1/2}$ and n is the refractive index of the material. In Fig. 2b, c, the surface artefacts created by the lenses are depicted. According to Fig. 2d [64], the AR structure used two different types of lenses with various diameters and apex heights.

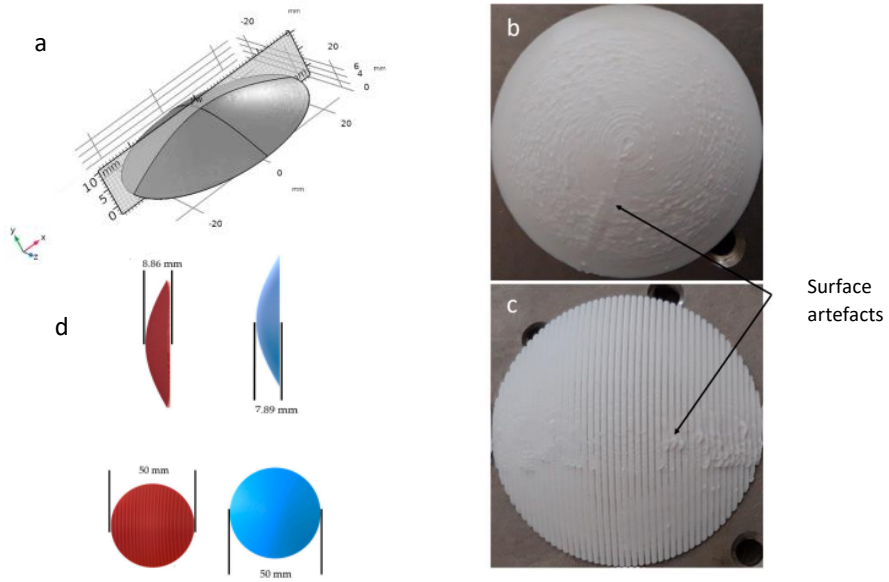

Fig 2 a) 3D model for printed PLA lenses and (b, c) surface artefacts (d) diameter and apex height of two types of lenses used in forming the AR structure [64]

3.3 Distortion in 3D printed lenses

A lens 3D printed entirely vertically may have some additional distortion, whereas a lens 3D printed horizontally may have layer line artefacts at the centre of the lens's axis. The clearest lenses were printed at a 30° angle to the build platform, with supports only placed around the edge, to prevent support marks on important lens surfaces. The projection micro-stereolithography (PSL) technique has been used to quickly create optical lenses for 3D printing. Three processes—manual sanding, automated sanding, dipping grayscale photo polymerization and meniscus coating processes—are used to polish lenses for optical clarity [48].

3.4 Sensing applications

Direct laser printing can create 3D-printed contact lenses with built-in microchannels at the edges for diagnostic reasons. [49, 50]. It has also been stated that a photodetector was created utilizing PET film and 3D printing [51]. An interferometric pressure sensor has also been constructed using a Fabry-Perot interferometer based on a tiny optical fibre [52]. DLP was once more used to produce an optical waveguide in a transparent photosensitive resin for a gas sensor [53]. It was possible to track finger flexion using a 3D-printed optical sensor that was based on the attenuation of light transmitted by crossed polarizers. [54]. The features of the 3D-printed optical elements may be improved using specific post-treatments, such as covering the samples with a liquid resin sheet of adequate thickness, curing them with UV light, and removing the uncured residues with isopropyl alcohol. Transmittance would rise as a result [55].

3.4 Polarizers

A polarising beam splitter has been manufactured using 3D printing at the end of a single-mode optical fibre [56]. Additionally, using 3D printing, a Fresnel Rhomb, a rhombohedral prism in

which incident light is twice reflected if it strikes at the proper angle, has been produced **[57]**. Due to this, there is a 90° phase shift between the two incident polarisation orientations. Optical spin splitters using spin-orbit optical vortex generators have been reported [58]. Convex spiral phase plates and dielectric meta surface birefringent optical retarders with outstanding polarisation conversion efficiencies were constructed using femtosecond 3D direct laser writing **[59, 60]**.

3.5 Metamaterials

The interaction of all three materials in a plasmonic metamaterial gel that can be printed in three dimensions and contains cellulose and gold nanorods in a liquid crystalline colloidal host results in polarization-dependent plasmonic properties, in this case by displaying different colours for different polarisation orientations **[61]**. For printed flexible substrates for rigid photonic elements and movable photonic structures, liquid crystal elastomers were employed **[62]**. A number of metamaterial surfaces with a range of capabilities for the optical and terahertz regions were produced via SLA printing **[63]**.

3D printing in biomaterials

Rapid tooling and multilayer micromanufacturing (AM) are promising applications of 3D printing, sometimes referred to as additive manufacturing. It has a wide range of uses in energy storage, filtration, and purification in addition to structural composites, thermal packaging, electrical devices, and biological implants. Vat polymerization, jetting, material extrusion, and powder bed fusion are a few 3D printing techniques. **[65]**. Nowadays, 3D printing is employed for the design and manufacture of scaffolds, which calls for the optimisation of mechanical characteristics, pore size, and interconnectivity. To determine the effective modulus that best matches the properties of bone, finite element modelling is used. By using 3D printing, bioceramics with magnetite nanoparticles were created, and non-linear bending and post-buckling properties were investigated. The Brazilian disc model's maximum rupture strength is expressed in terms of tensile strength P, diameter D, and thickness t. as $\sigma_r = \frac{2P}{\pi Dt}$ **[66]**.

The packaging and construction of biomedical devices like scaffolds, orthopaedic implants, and drug delivery systems frequently use the bioplastic poly-lactic acid (PLA). The 3D print was made using PLA filament. It is either heated to crystallise it or produced into a composite with woof flour because of its low mechanical properties in the amorphous state and its little potential for bio mimicry. Composites made from petroleum-based polymers and biological fillers can also be printed in 3D. Natural (alginate, gelatin, and collagen) Hyaluronic acid is employed in bioprinting, and synthetic polymers like PVA and PEG are used to create the bio-inks used in 3D printing. One bio-based resin made from soybeans can be produced optically in 3D without the use of a photo-initiator. In the fabrication procedure, a tabletop 3D printer and laser nanolithography were used. Made in an industrial line production service are checkered patterns **[67–69]**. Bone tissue engineering is a key area of application for 3D printing **[70].**

4. Summary

Biomedical systems are created utilising 3D printing processes like SLS, SLA, DLP, FFF, FDM, and ink-jet printing employing polymers, ceramics, and polymer ceramic composites like PC, PET, PLA, ABS, PZT, BTO, and PVDF. For high-frequency parts like RF coils in MRI and bio-monitoring equipment, dielectric parameters including the dielectric constant, tangent loss, and piezoelectric constant are crucial. Making biomedical prototypes involves employing a micro-lens array made of 3D-printed lenses, optical phantoms, contact lenses with built-in microchannels, rhombohedral prisms, etc. with the right optical properties.

References

1. G. E. Ryan, A. S. Pandit, and D. P. Apatsidis, Biomaterials, 29, 27, 3625– 3635, 2008.
2. H. N. Chia and B. M. Wu, 9, 4 2015.
3. C. Zhang, N. C. Anzalone, R. P. Faria, and J. M. Pearce PLoS ONE, 8, 3, e59840, 2013.
4. G. Comina, A. Suska, and D. Filippini, 14, no. 16, 2978–2982, 2014.
5. S. K. Moon et al Int J. Prec. Eng & Manufac - Green Technology, 1, 3, 223–228, 2014.

6. D. T. Pham and R. S. Gault, Int. J. Machine Tools and Manufac, 38, no. 10-11, 1257–1287, 1998.
7. P. S. P. Poh, M. P. Chhaya, F. M. Wunner et al. Adv Drug Delivery Rev, 107, 228–246, 2016.
8. Zeng Y et al J. Phy D: Appl Phy, 2021, 55(1), 013002.
9. Y. Zhu et al Add. Manufac 2022, 52, 102682
10. E. Udofia et al Add. Manufac 2022, 31, 100912
11. J. Agueda et al MRS Communications, 2021, 11:197–212
12. Han, Tao, et al. Sensors 19.7 (2019): 1706.
13. T Blachowicz et al e-Polymers 2021; 21: 549–565
14. T. Picha et al Res Agr. Eng, 69, 2023
15. D. Spolin et al Int. J. Adv. Manuf. Technol. (2014) 72:963-978.
16. E. MacDonald et al 2014, IEEE Access, vol.2, pp.234-2422014
17. S. Hayden et al IEEE Tran Dielec Elec Insul 2015, 2, 6, p.3543-3549
18. Castles, F., Isakov, D., Lui, A. et al. Sci Rep 6, 22714 (2016)
19. D. Kalas et al Polymers 2021, 13(21), 3702
20. C. Dichtl et al Adv Mater Sc & Eng 2017, 6913835.
21. B. Behzadnezhad et al J Magn Reson. 2018, 289, 113–121.
22. M.S. Boybay et al IEEE Trans. Instrum. Meas. 61 (2012) 3039–3046.
23. J. Baker-Jarvis et al IEEE Trans. Dielectr. Electr. Insul. 5 (1998) 571–577.
24. Kumar V et al Proc. Inst Mechl Eng H: J Eng Med. 2022; 236(8):1057-1069
25. Rashid, S., et al (2019). IEEE Antennas and Wireless Propagation Letters, 18(4), 626-630.
26. Bicer, M.B. Phys Eng Sci Med 44, 1175–1186 (2021)
27. Sarjoghian S et al 2021 IEEE Trans Antennas Propag 69:64–73
28. Sarjoghian S et al. IEEE Access 7 (2019): 94977-94985.
29. Wang Z et al 2020 Nano Energy 73 104737
30. Liang Y 2021 J. Memb. Sci. 618 118709
31. Reiser A et al 2019, Nat. Commun.10 1–8
32. Cooperstein I, 2018 Adv. Mater. Interfaces 5 1800996
33. Khoo Z X et al 2015 Virtual Phys. Prototype. 10 103–22
34. Jiang L et al 2019 Adv. Funct. Mater. 29 1902522
35. Wei H et al 2018 J. Mater. Chem. C 6 12446–67
36. Wei X et al 2020, J. Eur. Ceram. Soc. 40 5423–30
37. Tandon B 2018 Acta Biomater. 73 1–20
38. Khare D 2020 Biomaterials 258 120280
39. Shuai C et al 2020 Colloids Surf. B 185 110587
40. Polley C 2020 Materials 13 1773
41. Liu W et al 2020 J. Biomater. Appl. 35 544–52
42. Tariverdian T 2019 Ceramics Int. 45 14029–38
43. P. Diep et al Biomed Opt. Exp. 2015, 6, 4212–4220
44. Liu JH, Chen XD. Optik. 2019;194: 163119.
45. Lo WC, Tsai KM, Hsieh CY. Int J Adv Manuf Technol. 2009; 41: 885–96.
46. Li YL, Li TH, Jiao GH, Hu BW, Huo JM, Wang LL. Optik.2007;118:395–401
47. Assefa BG, et al Opt Exp. 2019;27:12630–37
48. Shao, G, Hai, R, Sun C., Adv. Optical Mater. 2020, 8, 1901646
49. Alam F et al.. ACS Biomater Sci Eng. 2021;7(2):794–803.
50. Alam F, Elsherif M, AlQattan B, Ali M, Ahmed IMG, Salih A,et al. Adv Eng Mater. 2021; 23: 2000941.
51. Park SH, Su R, Jeong J, Guo SZ, Qiu K, Joung D, et al. Adv Mater. 2018;30(40):1803980.
52. Wei HM, Chen MQ, Krishnaswamy S. Appl Opt. 2020;59(7):2173–88.
53. Swargiary K et al Appl Opt. 2020;59(1):122–88.
54. Wang LF, Meydan T, Williams P. IEEE Sens J. 2017;17(6):1937–44
55. Szukalski A, et al. Proc SPIE. 2019; 10915:1091503.
56. Hahn V, Kalt S, Sridharan GM, Wegener M, Bhattacharya S. Opt Exp. 2018;26(25):33148–57
57. Bertoncini A, Liberale C. IEEE Photonics Technol Lett. 2018;30(21):1882–55.
58. Wang XW et al Appl Phys Lett. 2017; 110:181101.
59. Varapnickas S et al Appl Phys Lett. 2021;118:151104.
60. Liu C, Hu C, Wei D, Chen M, Shi J, Wang H, et al.Micromach.2020;11(8):771.
61. Hess AJ, ACS Omega.2019;4(24):20558–63.
62. Woska S, Optical Mater Exp. 2020;10(11):2928–43.
63. Sadeqi A Microsyst Nanoeng. 2019;5:16.
64. Friel RJ, Gerling-Gerdin M, Nilsson E, Andreasson BP.*Designs*. 2019; 3(2):28
65. W. Xu, S. JambhulkarComposites Part B 223 (2021): 109102,
66. A. Elghazel, R. Taktak and J. Bouaziz Intech Open, (2016)
67. Dries Vaes and Peter Van Puyvelde, Progress in Polymer Science 118 (2021):101411,
68. V. I. Putlyaev, P. V. Yevdokimov, Inorganic Materials: Applied Research 10 (2019): 1101.

69. A. Jasemi et al Ceramics International 48 (2022): 1314.
70. M. M. Germaini, ' S. Belhabib 130 (2020) 100963.